Journal of Materials Chemistry C

Accepted Manuscript

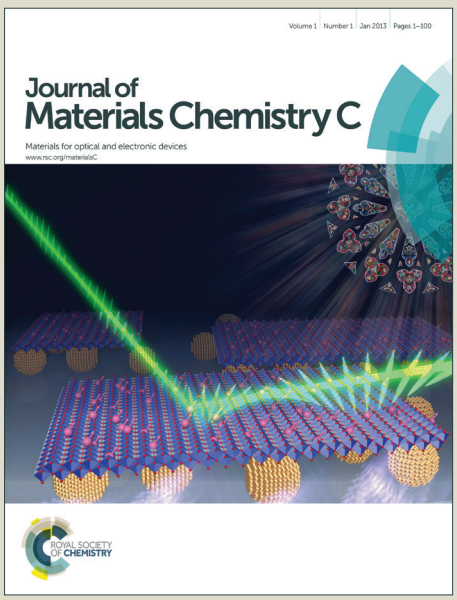

ROYAL SOCIETY OF CHEMISTRY

www.rsc.org/materialsC

Journal of Materials Chemistry C RSCPublishing

ARTICLE

Chemical trends of electronic and optical properties of ns^2 ions in halides

Cite this: DOI: 10.1039/xoxxoooooox

M. H. Du[a]

Received ooth January 2014,
Accepted

DOI: 10.1039/xoxxoooooox

www.rsc.org/

Heavy 6p and 5p ions in groups IIIB, IVB, and VB (Tl, Pb, Be, In, Sn, Sb) are multivalent ions, which act as electron and hole traps and radiative recombination centers in many wide band gap materials. In this paper, Tl^+ as a prototypical ns^2 ion (ns^2 ions here refer to 6p and 5p ions with outer electronic configuration of ns^2) is studied as luminescent centers in alkali halides. Density functional calculations reveal the chemical trend that determines the luminescence mechanism in ns^2-ion activated alkali halides. The activator-halogen hybridization strength and the ionicity of the host material strongly affect the positions of the activator levels relative to the valence and conduction band edges. This determines whether the radiative recombination occurs within the activator ion or involves the hole polaron, or the V_k center. Strategies for exploring different combinations of host materials and activators for desired luminescence mechanisms are discussed. The insight obtained in this work will help the search and the design of more efficient scintillators and phosphors.

I. Introduction

Many inorganic and organic semiconducting and insulating materials can emit photons under external excitation (e.g., electromagnetic waves, chemical reactions, heat, etc.). Luminescence of materials when excited by photons or ionizing radiation is the foundation for numerous technologies, such as energy efficient lighting (fluorescent lamps and white LEDs), laser, medical imaging, and nuclear materials detection. [1, 2, 3]

Efficient luminescence in inorganic semiconductors and insulators usually relies on the localization of excited electrons and holes at certain impurities, which act as luminescence centers. Such impurity is the so-called activator, which can trap electrons and holes for efficient radiative recombination and is the essential component of a phosphor or scintillator material. The commonly used activators are typically multivalent ions, which can insert multiple electronic states inside the band gap of the host material. [4 5] These gap states trap electrons and holes, leading to radiative recombination. Good examples of the multivalent ions that can act as luminescent centers are rare-earth (e.g., Ce^{3+}, Eu^{2+}) [6 7 8 9 10 11] and transition metal ions (e.g., Cr^{3+}, Mn^{4+}).[12, 13, 14, 15, 16, 17]

Besides rare-earth and transition-metal ions, a number of heavy 6p (Tl, Pb, Bi) and 5p (In, Sn, Sb) ions are also important multivalent ions, which act as luminescent centers in many materials. These ions in their ground states all have the outer electronic configuration of ns^2 and are therefore called ns^2 ion. The hybridization between the ns and np states of these ions and the host states can create ns- and np-derived electronic states inside the band gap of the host material. These gap states give rise to many sub-band-gap optical transitions, which can be between the ns and the np levels, [18 19 20] between np levels (due to the spin-orbit splitting of the np levels), [21, 22, 23, 24, 25, 26, 27] or between the np level and the native defects.[2, 28, 29] Tl^+ doped NaI and CsI are two important high-performance scintillators that have been widely used for radiation detection.[2] The 6p→6s transition is responsible for the Tl emission in NaI:Tl^+.[18,19,20] The emission in CsI:Tl^+ appear to be related to both the hole polaron (V_k center) and the electron trapped at Tl, or Tl-bound exciton. [2,28,29] The optical transitions between the 6p states of Bi^{2+} have also been reported in various materials, leading to emission wavelength in the range of 600-700 nm, which is useful for red phosphors in fluorescent lamps and white LEDs,[21,22,23,24] Many 6p and 5p ions at low valence states (such as Bi^+) can also produce broad-band near IR emission, which is useful for wideband optical amplification and lasers.[25,26,27] The complex luminescence properties of the 6p and 5p dopants in various host materials require detailed understanding of dopant-induced gap states and their interaction with the host states.

The optical transitions between the ns and np states of a ns^2 ion are usually interpreted and modeled by using Seitz model.[30] The Seitz model is based on a two-electron picture, in which the ground state (ns^2) is a singlet $^1S_0$ state and the excited states (nsnp) consist of $^3P_0$, $^3P_1$, $^3P_2$ triplet states and a $^1P_1$ singlet state (in the ascending order in energy). The often observed A, B, C bands in the optical absorption spectra are usually interpreted as the $^1S_0$→$^3P_1$, $^3P_2$, $^1P_1$ transitions, respectively.[19] The A and C bands are the two strong absorption bands. The C-band ($^1S_0$→$^1P_1$) transition is spin-allowed. The A-band ($^1S_0$→$^3P_1$) transition is spin-forbidden but is still strong, especially for heavy 6p ions, due to the spin-orbit coupling between the $^3P_1$ and the $^1P_1$ states. Emission is more complicated involving lattice polarization in the emitting states. More details on the optical transitions in ns^2 ions based on the Seitz model can be found in several review articles.[18,19,20]

The extensions of the Seitz model based on pure ionic model[31, 32] and molecular orbit (MO) theory[33, 34] have been used to quantitatively calculate various properties related to the optical transitions (e.g., absorption and emission energies, line shapes,

intensity ratio, etc.). The MO calculations showed reasonable results for some systems when compared with the spectroscopic data.[33, 34] However, these calculations, which treat only one ns^2 ion and six nearest-neighbor halogen ions quantum mechanically, lack the description of the host band structure and the accurate structural relaxation. As discussed above, many optical transitions between ns, np, and native defect levels can occur. Whether the specific emission between the nsnp and ns^2 states as described by the Seitz model can occur depends on the positions of the ns and np states relative the host band edges. The knowledge of the electronic structure of both the host and the activator is needed to understand the different scintillation mechanisms observed in different host materials (e.g., NaI:Tl vs. CsI:Tl). Sufficiently accurate structural relaxation is important for incorporating correct hybridization strength between the activator and its ligands in the calculations. The different hybridization strengths in different hosts determine the chemical trend of the activator-induced gap levels relative to the host bands. This is important for the understanding of the luminescence mechanisms in different hosts and the search of new host-activator combinations with desirable scintillation properties.

In this paper, density functional calculations based on density functional theory (DFT) are used to study the electronic and optical properties of Tl^+ in alkali halides. Tl^+ ion is used as a prototypical ns^2 ion. The objective of this work is to understand how the activator-ligand hybridization and the ionicity of the host material affect the activator level positions and the luminescence mechanism. The results show that the strong hybridization tends to lead to np→ns emission whereas the weak hybridization may activate the np→V_k emission. The relatively low scintillation efficiency of Pb^{2+}, Bi^{3+}, and some other ns^2 ions[2, 35] may be remedied if an optimal host-activator combination can be found to invoke the luminescence mechanism that involves the hole polaron, similar to that in CsI:Tl. This insight may help the search of new small-band-gap materials with efficient long-wave-length emission. The chemical trend discovered for Tl^+ ion should also apply to other ns^2 ions, such as Pb^{2+} and Bi^{3+}. The electronic structure of the ns^2 ions presented in this paper also serves as the starting point for the future studies of these ions with different oxidation states involving electronic configuration of ns^2np (e.g., Tl^0 and Bi^{2+}) or ns^2np^2 (e.g., Bi^+).

II. Computational Methods

Density functional calculations were performed using the VASP codes.[36, 37] Perdew-Burke-Ernzerhof (PBE)[38] and hybrid PBE0 exchange-correlation functionals[39] were both employed. The results on structures and electron and hole trapping energies and levels were obtained by using hybrid functional calculations. The fraction of the Hartree-Fock exchange was tuned to reproduce the experimental band gaps of various halides, as shown in Table I. The hybrid density functional methods have been shown to improve results on the band gap, defects, and the charge localization in semiconductors.[40 41, 42, 43, 44, 45, 46] The PBE functionals were used for density of states (DOS) calculations because it is very time-consuming to produce high-quality DOS figures, which require the use of a large number of k points, by using the hybrid functional calculations. Spin-orbit coupling is included in all calculations.

The electron-ion interactions were described using projector augmented wave potentials.[36, 47] The valence wavefunctions were expanded in a plane-wave basis. The cutoff energies are 260 eV for NaI, KI, and KCl, and 237 eV for RbI and CsI. A 64-atom and a 54-atom cubic supercell were used for rocksalt and simple-cubic structures, respectively, in defect- and dopant-level calculations. A 2×2×2 and a 6×6×6 grids were used for the k-point sampling of the Brillouin zone for defect and DOS calculations, respectively. All the atoms were relaxed to minimize the Feynman-Hellmann forces to below 0.05 eV/Å.

Table I. The fractions of Hartree-Fock exchange (α) used in the PBE0 calculations and the calculated band gaps, which are compared to the experimental band gaps[2] shown in parentheses. Both simple cubic (ground state) and rocksalt CsI are considered.

	NaI	KI	RbI	CsI (RS)	CsI (SC)
α	0.37	0.39	0.40	0.37	0.37
E_g (eV)	5.81 (5.9)	6.23 (6.3)	6.23 (6.3)	6.28	6.05 (6.1)

The charge transition level $\varepsilon(q/q')$, induced by activators or polarons, is determined by the Fermi level (ε_f) at which the formation energies of the activator or the defect with charge states q and q' are equal to each other. $\varepsilon(q/q')$ can be calculated using

$$\varepsilon(q/q') = \frac{E_{D,q'} - E_{D,q}}{q - q'}, \quad (1)$$

where $E_{D,q}$ ($E_{D,q'}$) is the total energy of the supercell that contains the relaxed structure of a defect at charge state q (q'). Corrections to the charge transition level due to potential alignment (between the host and the charged defect supercell) and image charge interaction were applied.[48] Details on the calculations of defect formation energies and transition levels can be found in Refs. 48, 49 and 50.

III. Results

Figure 1(a) shows the DOS for NaI:Tl calculated using the PBE functionals. The valence band is predominantly of I-5p character. Both Tl 6s and 6p states hybridize with the I-5p states. The resulting Tl-6s bonding level is below the valence band while the anti-bonding Tl-6s* level is above the valence band maximum (VBM) as shown in Fig. 1(a). The bonding and anti-bonding characters of the Tl-6s and Tl-6s* states are shown by their wavefunctions as shown in Fig. 2(a) and (b). Hybrid functional calculations show that the Tl-6s* eigenstate is about 0.4 eV above the VBM (see Table II). The Tl-6s* level can trap a hole with the Tl^+/Tl^{2+} transition level located at 1.1 eV above the VBM (Fig. 3(a)). The trapping of a hole reduces the Tl-I bond length from 3.37 Å to 3.17 Å.

Table II. Single-particle levels (eigenlevels) of Tl-6s* and 6p* relative to the VBM and the CBM, respectively, in NaI, KI, RbI, rocksalt CsI (RS), and simple-cubic CsI (SC). These are calculated using hybrid functionals. The units are in eV.

	NaI	KI	RbI	CsI (RS)	CsI (SC)
ε(Tl-6s*) – ε_v	0.40	0.31	0.24	0.31	<0
ε(Tl-6p*) – ε_c	0.29	0.18	0.15	-0.10	– 0.76

The six Tl-6p* levels are split by the spin-orbit coupling to two lower- and four higher-lying levels. The two lower states are more localized and near the CBM while the four higher states have relatively stronger mixing with the host conduction band states. Hybrid functional calculations show that the lowest Tl-6p* single-particle level is slightly above the conduction band minimum (CBM) by 0.29 eV for Tl^+ (see Table II). Upon trapping a hole, the empty Tl-6p* level remains above the CBM for Tl^{2+}. However, the lowest

Tl-6p* level of Tl^{2+}, once occupied, descends below the CBM to stabilize the electron trap, $Tl^{+,*}$. The Tl-I bond length increases from 3.17 Å for Tl^{2+} to 3.32 Å for $Tl^{+,*}$ at octahedral structure. $Tl^{+,*}$ undergoes a Jahn-Teller distortion to assume a tetragonal structure with four short and two long Tl-I bonds. The bond lengths of the short and long Tl-I bonds are 3.25 and 3.47 Å, respectively. This result is consistent with the experimentally observed tetragonally polarized emission in ns^2 ion activated alkali halides.[19] The total energy is calculated to be lowered by 0.6 eV upon the trapping of one conduction band electron by Tl^{2+} at the Tl-6p* level ($Tl^{2+} + e^-_{CB} \rightarrow Tl^{+,*}$) (see Fig. 3(a)). [The total energy of $Tl^{+,*}$ (Tl 6s6p state) is calculated using the constrained DFT method, where a hole and an electron are forced into the Tl-6s* and Tl-6p* levels, respectively.]

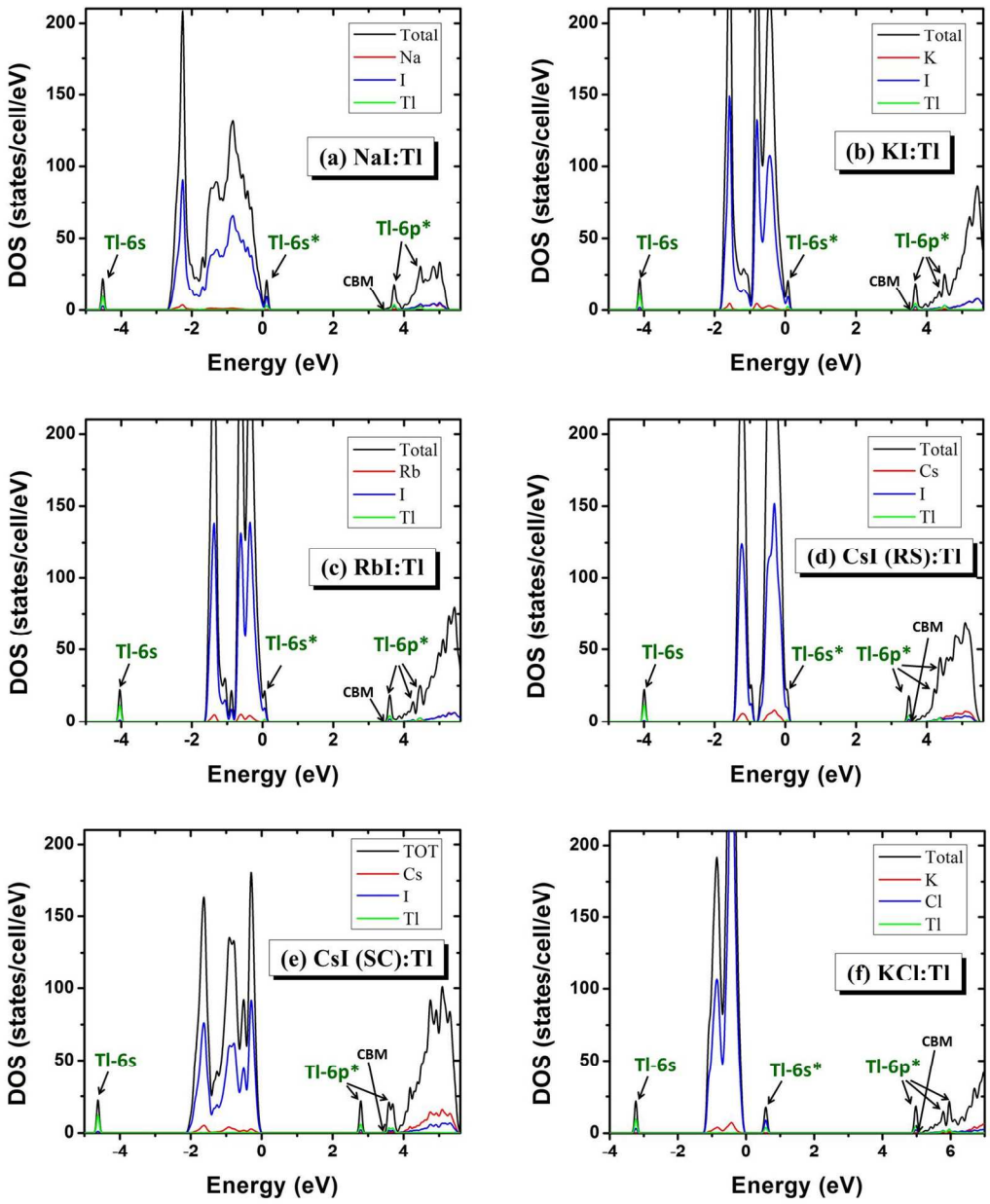

Figure 1. (Color online) Density of states (DOS) for Tl doped (a) NaI, (b) KI, (c) RbI, (d) CsI (rocksalt), (e) CsI (simple cubic), and (f) KCl. The energy of VBM is set at zero. Note that the band gaps are underestimated due to the use of PBE functionals. The Gaussian broadening of 0.05 eV was used for all the DOS calculations.

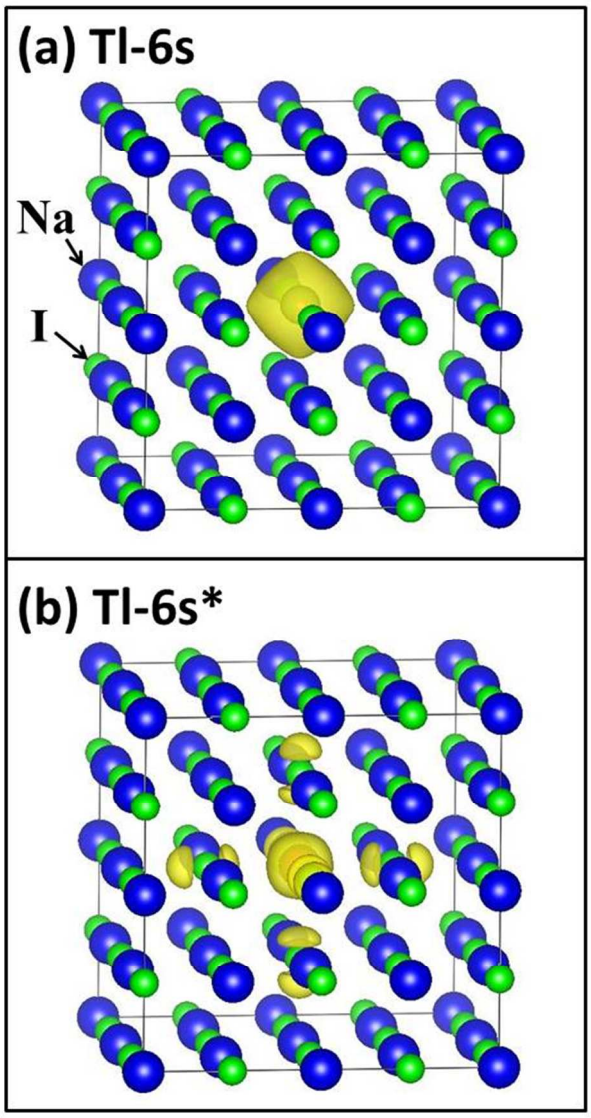

Figure 2. (Color online) Charge density contour (0.0015 e/bohr^3) for the (a) Tl-6s and (b) Tl-6s* states (see Fig. 1(a)) in NaI:Tl. The blue and green balls represent Na and I ions respectively. The Tl ion is at the center of the supercell surrounded by the Tl-6s or Tl-6s* wavefunction (yellow isodensity surface).

The optical absorption energy is calculated following the Franck-Condon principle. The energy difference between the $Tl^{+,*}$ (Tl 6s6p) excited state and the Tl^+ (Tl $6s^2$) ground state calculated using the Tl^+ ground-state structure is 4.06 eV, reasonably close to the experimentally observed A-band absorption energy of 4.35 eV.[2, 51] The relaxation of the $Tl^{+,*}$ (Tl 6s6p) excited state leads to tetragonal distortion as described above. The emission energy calculated by taking the energy difference between the excited and ground states of Tl^+ at the tetragonally distorted excited state structure is 3.89 eV. However, the experimentally observed emission energy is 2.95 eV,[2, 51] having a very large Stokes shift of 1.4 eV. The failure of the DFT calculations to reproduce such a Stokes shift is likely due to the fact that DFT is a ground-state theory and is therefore not reliable in finding the energy minimum at the excited state.

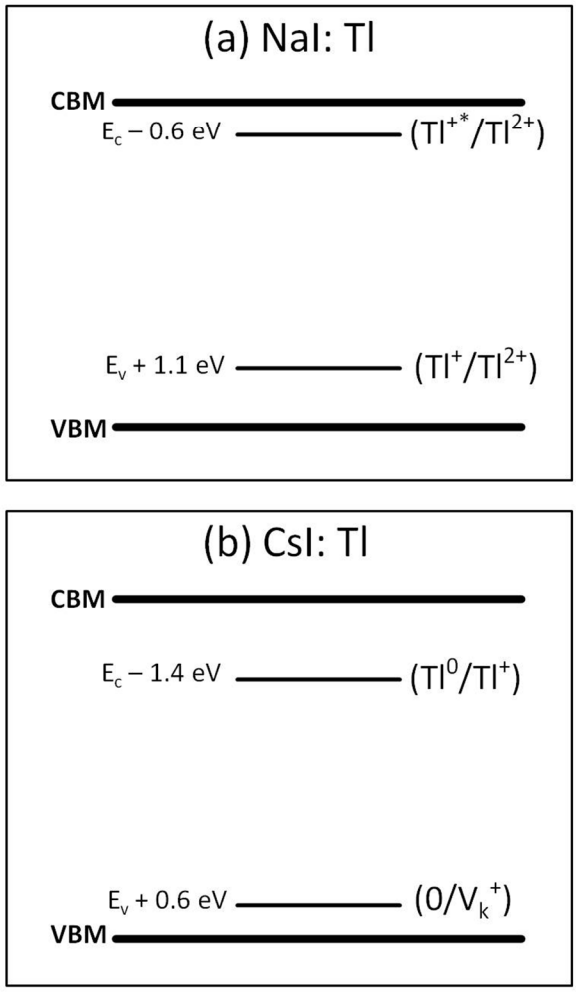

Figure 3. Hole and electron trapping levels in (a) NaI:Tl and (b) CsI:Tl. In (a), it is assumed that the hole is trapped first by Tl^+ at the Tl-6s* level [(Tl^+/Tl^{2+}) transition level] and then the electron is trapped by Tl^{2+} at the Tl-6p* level [(Tl^{+*}/Tl^{2+}) transition level]. In (b), the electron and hole are trapped separately by Tl^+ and the V_k center.

The result that the lowest single-particle Tl-6p* level of Tl^+ and Tl^{2+} in NaI:Tl is slightly above the CBM suggests that the exothermic electron trapping at Tl-6p* may involve a small kinetic barrier. This can explain why Tl^+ in NaI usually captures a hole before capturing an electron despite that an electron has higher mobility than a hole in NaI.[2] The single-particle Tl-6p* level relative to the CBM in KI:Tl is lower than that in NaI:Tl (see Table II), which suggests a lower kinetic barrier for electron trapping at Tl in KI than in NaI. This is consistent with the experimental observation that the probability for Tl in KI to capture an electron before capturing a hole is higher than that in NaI.[2]

Figure 1(b) shows the DOS for KI:Tl. Compared to NaI, the I-I distance in KI is longer and thus the valence band is narrower. The Tl-I bond length in KI (3.55 Å) is also longer than that in NaI (3.37 Å) (see Table III), thereby reducing the Tl-I hybridization strength. The reduction of the Tl-I hybridization becomes more evident in the DOS figures for RbI and rocksalt CsI. As shown in Figs. 1(c) and (d), the Tl-6s* level gradually merge with the valence band when the Tl-I bond length increases. From Fig. 1(a) to Fig. 1(d), it can be seen that the energy separation between the Tl-6s bonding and Tl-6s*

antibonding states decreases with increasing Tl-I bond length (weaker hybridization).

CsI has a different crystal structure [simple cubic (SC) CsCl structure] than that of the other alkali metal iodides [rocksalt (RS) NaCl structure]. (However, the DOS for RS CsI (Fig. 1(d)) is also calculated for comparison with other alkali metal iodides of RS structures.) In SC CsI, there is a structural distortion for Tl_{Cs} because Tl^+ is significantly smaller than Cs^+ in size. (The ionic radii for Tl^+ and Cs^+ in eight-fold coordination are 1.73 and 1.88 Å, respectively.) The Tl^+ moves off-center towards four of the eight nearest-neighbor I^- ions, assuming a structure with roughly four-fold rotational symmetry. The four short and the four long Tl-I bond lengths are 3.67 and 4.19 Å in average. The Tl-I bond length shown in Table III is the average of the short and long Tl-I bond lengths. As a result of the further reduced Tl-I hybridization in CsI:Tl, the Tl-6s* state resonates with the valence band and disappears from the band gap, as shown in Fig. 1(e). The weak Tl-I hybridization in CsI also lowers the Tl-6p* level, which resides deep inside the band gap. This is in contrast to NaI:Tl, KI:Tl, and RbI:Tl, where the Tl-6p* level is near the CBM.

Table III. The calculated Tl-I bond lengths and the nearest-neighbor I-I distances, in NaI:Tl, KI:Tl, RbI:Tl, CsI:Tl. Tl_{Cs} in simple-cubic (SC) CsI undergoes a structural distortion. The Tl-I bond length shown for CsI (SC) is the average over all Tl-I bonds.

	NaI	KI	RbI	CsI (SC)
Tl-I bond length (Å)	3.37	3.55	3.63	3.93
I-I distance (Å)	4.57	5.02	5.24	4.60

The Tl-I bond lengths and the I-I distances are shown in Table III for NaI, KI, RbI, and CsI (SC). CsI (SC) has the longest Tl-I bond length and a relatively short I-I distance close to that of NaI. Therefore, CsI (SC) has the weakest Tl-I hybridization and a relatively wide valence band among the alkali halides studied in this work. These explains the disappearance of the Tl-6s* level from the CsI band gap.

The unique electronic structure for CsI:Tl determines that the luminescence mechanism for CsI is different from that of many other alkali halides. The emission from Tl-activated alkali halides is typically of the type of Tl 6p*→6s* transition. But the emission from the CsI:Tl is shown to be involved with the self-trapped hole or the V_k center. [2,28,29] The hybrid functional calculations show that the electron trapping at the Tl-6p* level ($Tl^+ + e^- \rightarrow Tl^0$) and the hole self-trapping at a V_k center lower the total energy by 1.4 and 0.6 eV, respectively (Fig.3 (b)). The trapping of an electron increases the average Tl-I bond length from 3.93 Å for Tl^+ to 4.14 Å for Tl^0. The off-centering distortion of Tl_{Cs} is also reduced. The four short and four long Tl-I bonds have average bond lengths of 4.05 and 4.22 Å for Tl^0, respectively, compared with those of 3.67 and 4.19 Å for Tl^+. In the V_k center, two nearest-neighbor I^- ions move close to each other, forming a I_2^- molecule. The distance between the two I ions is reduced from 4.60 Å to 3.22 Å, in good agreement with a previous PBE0 calculation.[52] Accurately describing charge localization in small polarons and V_k centers is a challenging problem for DFT within the local density or generalized gradient approximation due to the self-interaction error. Methods that incorporate non-local Fock exchange (as done in the present work) or an on-site potential have been shown to be effective in stabilizing localized holes at small polarons in wide-gap materials. [40 42 45 53]

Electron paramagnetic resonance experiments showed that the rate of formation of the V_k centers is increased orders of magnitudes by the Tl doping in some alkali halides due to electron trapping by Tl^+.[54] The V_k center can migrate and binds with Tl^0.[28] The emission from CsI:Tl is likely due to Tl-bound excitons. [29] Such emission is denoted 6p*→ V_k in this paper.

The calculations presented above are focused on Tl-doped iodides. For Tl-doped bromides and chlorides, the valence band is lower, narrower, and closer to the Tl-6s level. In KCl:Tl^+, the hybridization between the Tl-6s state and the Cl 3p states is more confined within the nearest-neighbor halogen ions to Tl. The anti-bonding Tl-6s* state is more localized in Tl-doped chlorides than in iodides because the Cl 3p states are more localized than the I 5p states (narrower valence band). The DOS for KCl:Tl^+ shows a deep Tl-6s* level inside the band gap (Fig. 1(f)).

IV. Discussion

The results in Sec. III show that both the hybridization strength between the Tl and its ligands and the ionicity of the host material have strong impact on the positions of the Tl-induced electronic states relative to the band edges. The Tl 6s level is typically below the valence band while the Tl 6p levels are above the valence band.[55, 56] The Tl-halogen hybridization (mainly within the nearest neighbors) produces two antibonding levels, i.e., Tl-6s* and -6p* levels, as schematically shown in Fig. 4. Strong/weak Tl-halogen hybridization should result in high/lowTl-6s* and Tl-6p* levels relative to the band edges. Hybridization among halogen ions is also important. For instance, strong halogen-halogen hybridization widens the valence band and lower the positions of the Tl-6s* and Tl-6p* levels relative to the VBM. The interplay of the Tl-halogen and halogen-halogen hybridization determines the positions of the Tl-6s* and -6p* levels relative to the band edges.

A combination of the strong Tl-halogen and weak halogen-halogen hybridization could result in the scenario depicted in Fig. 4(a), where both Tl-6s* and -6p* levels are inside the band gap and act as hole and electron traps, respectively, leading to radiative recombination. On the other hand, weak Tl-halogen hybridization combined with strong halogen-halogen hybridization may lead to the scenario depicted in Fig. 4(b), where only the Tl-6p* level is inside the band gap to trap electrons. Nevertheless, efficient luminescence is still possible in the scenario of Fig. 4(b) because the hole can be localized by a small hole polaron bound to the Tl^0 electron trap, leading to efficient radiative recombination. The emissions in NaI:Tl and CsI:Tl can be categorized into the scenarios depicted in Figs. 4(a) and (b), respectively.

Among many ns^2 ions that are activators in halide scintillators, such as In^+, Ga^+, Tl^+, Ge^{2+}, Sn^{2+}, Pb^{2+}, and Bi^{3+},[19] Tl^+ appears to be most efficient. Others often suffers from slow scintillation decay, strong afterglow, or low quantum yield. [2, 57, 58] Pb^{2+} and Bi^{3+} are the heaviest ions among the ns^2 ions, enabling strong spin-orbit coupling and more efficient $^3P_1 \rightarrow {}^1S_0$ emission. But a large energy separation between the lowest excited state $^3P_0$ and the $^3P_1$ states can also result from the strong spin-orbit splitting and reduce the electron population on the radiative $^3P_1$ state.[57]

Many previous experiments on Pb and Bi activated phosphors and scintillators involve fluoride or oxide-based large-band-gap host materials,[57, 58, 59, 60, 61, 62] which have narrow valence band width and low VBM.[63] This may lead to the electronic structure depicted in Fig. 3(a) and the emission consistent with the Seitz model, i.e., the 6p*→6s* emission. This is confirmed in $LiCaAlF_6$:Pb^{2+}, where both Pb 6s* and 6p* levels are found to be deep inside the band gap according to the hybrid functional calculations (not shown). It is possible that the 6p*→6s* transition in Pb^{2+} and Bi^{3+} is not efficient due to reasons such as the large energy separation between the $^3P_0$

and $^3P_1$ levels. However, the efficiency of the 6p*→V_k type of emission has not been studied in Pb^{2+} and Bi^{3+} activated materials. Since the efficiency of the 6p*→V_k emission is reasonably good in CsI:Tl, it should be of interest to explore ways to activate the same emission mechanism in Pb^{2+}, Bi^{3+}, and other ns^2-ion activated materials. The key to activate such emission mechanism is to have weak activator-anion hybridization and strong anion-anion hybridization as is the case for CsI:Tl. The weak activator-anion hybridization is particularly important for removing the ns* level from the band gap. This requires the size of the native cation to be large relative to that of the activator ion. For scintillators, a short nearest-neighbor anion-anion distance is also important for fast hole transport towards activators, which enables fast scintillation. The approach outlined above may open new routes of exploring low-band-gap materials for high-light-yield scintillators and phosphors.

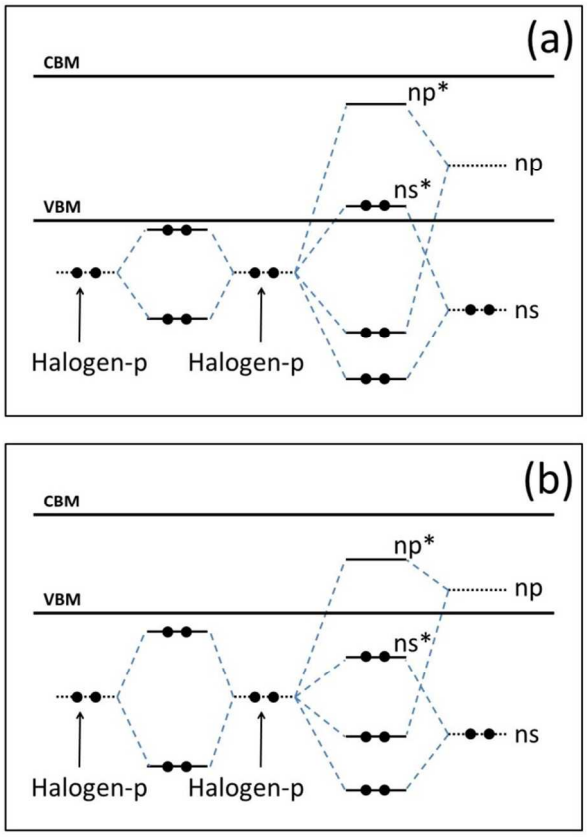

Figure 4. Schematic diagram of hybridization between the ns^2 and the halogen ions. In (a), the hybridization between the ns^2 and the halogen ion is relatively strong while the hybridization between the halogen-p states is relatively weak. In (b), the hybridization between the ns^2 and the halogen ion is relatively weak while the hybridization between the halogen-p states is relatively strong.

The light yield of some of the current state-of-the-art scintillators is already close to their respective theoretical limits, which suggests that improving crystal quality may have only limited upside potential on the light yield. Further reducing the band gap should in principle lead to higher light yield. However, a small band gap may not be able to accommodate both the electron- and hole-trapping levels of the activator, such as the case for LaI_3:Ce.[64, 65] Therefore, exploring the np*→V_k emission in ns^2-ion activated small-band-gap materials should be of interest for searching high-light-yield scintillators and phosphors because only the electron trapping level (np*) of the activator is required to be inside the band gap. For example, LaI_3:Bi^{3+} may be interesting as a potential scintillator because the electronic structure of Bi^{3+} in LaI_3 is similar to that of Tl^+ in CsI with a 6p* level but no 6s* level in the band gap according to our calculations.

V. Conclusions

This work employs density functional calculations to gain understanding on how the material chemistry affects the luminescence mechanism in ns^2-ion-activated halides. In the series of Tl activated NaI, KI, RbI, and CsI, the increasing Tl-I bond length decreases the Tl-I hybridization strength and lowers the Tl-6s* anti-bonding level. In the case of relatively strong Tl-I hybridization (e.g., NaI:Tl), the Tl-6s* level resides above the VBM and leads to the 6p*→6s* emission. When the Tl-I hybridization is weak, the Tl-6s* level disappears from the band gap and the emission is of the type of 6p*→V_k transition, which is the case for CsI:Tl. The emission of the ns^2 ions has usually been explained in the past based on the assumption of the 6p*→6s* emission. The insight obtained in this work can be useful for the search and design of new combinations of the host material and the ns^2 ion, which exhibit efficient 6p*→V_k emission, by tuning both the hybridization strength between the ns^2 ion and its ligands and the ionicity of the host material. This opens a new route for searching high-light-yield low-bandgap scintillators and phosphors. The electronic structure of the ns^2 ions presented in this paper serves as the starting point for the future studies of the heavy 6p and 5p ions with different oxidation states involving electronic configuration of ns^2np (e.g., Bi^{2+}) or ns^2np^2 (e.g., Bi^+), which have great potential for various optics applications, such as fluorescent lighting, optical amplification, and lasers.

Acknowledgements

The author is grateful for the stimulating discussion with W. Beall Fowler, Zane W. Bell and David J. Singh. This work was supported by the Department of Energy, Basic Energy Sciences, Materials Sciences and Engineering Division.

Notes and references

[a] Materials Science & Technology Division, Oak Ridge, TN 37831, USA

[1] G. Blasse and B. C. Grabmaier, "Luminescent Materials", Springer-Verlag, Berlin (1994).
[2] Piotr A. Rodnyi, "Physical Processes in inorganic scintillators", CRC Press, Boca Raton (1997).
[3] J. B. Birks, "The theory and practice of scintillation counting", Pergamon Press Ltd. (1964).
[4] K. Biswas and M. –H. Du, Phys. Rev. B, **86**, 014102 (2012).

[5] M. –H. Du and K. Biswas, J. Lumin. **143**, 710 (2013).
[6] A. A. Setlur, R. J. Lyons, J. E. Murphy, N. P. Kumar, and M. S. Kishore, ECS J. Solid State Sci. Tech. **2**, R3059 (2013).
[7] M. D. Birowosuto and P. Dorenbos, Phys. Stat. Sol. A **206**, 9 (2009).
[8] P. Dorenbos, J. Lumin. **91**, 91 (2000).
[9] P. Dorenbos, J. Lumin. **104**, 239 (2003).
[10] N. J. Cherepy, S. A. Payne, S. J. Asztalos, G. Hull, J. D. Kuntz, T. Niedermayr, S. Pimputkar, J. J. Roberts, R. D. Sanner, T. M. Tillotson, E. van Loef, C. M. Wilson, K. S. Shah, U. N. Roy, R. Hawrami, A. Burger, L. A. Boatner, W. –S. Choong, and W. W. Moses, IEEE Trans. Nucl. Sci. **56**, 873 (2009).
[11] W. W. Moses, Nucl. Instrum. Met. Phys. Res. A **487**, 123 (2002).
[12] M. H. Du, J. Mater. Chem. C 2014 DOI:10.1039/c4tc00031e.
[13] M. G. Brik, A. M. Srivastava, J. Lumin. **133**, 69 (2013).
[14] J. McKittrick, M. E. Hannah, A. Piquette, J. K. Han, J. I. Choi, M. Anc, M. Galvez, H. Lugauer, J. B. Talbot, and K. C. Mishra, ECS J. Solid State Sci. Tech. **2**, R3119 (2013).
[15] M. G. Brik and A. M. Srivastava, Opt. Mater. **35**, 1776 (2013).
[16] S. Geschwind, P. Kisliuk, M. P. Klein, J. P. Remeika, D. L. Wood, Phys. Rev. **126**, 1684 (1962).
[17] M. A. Noginov, G. B. Loutts, N. Noginova, S. Hurling, and S. Kück, Phys. Rev. B **61**, 1884 (2000).
[18] P. W. M. Jacobs, J. Phys. Chem. Sol. **52**, 35 (1991).
[19] A. Ranfagni, D. Mugnai, M. Bacci, G. Viliani, and M. P. Fontana, Adv. Phys. **32**, 823 (1983).
[20] W. Beall Fowler, "Physics of color centers", edited by W. Beall Fowler, Academic Press Inc., New York (1968).
[21] G. Blasse, A. Meijerink, M. Nomes, and J. Zuidema, J. Phys. Chem. Solids **55**, 171 (1994).
[22] A. M. Srivastava, J. Lumin. **78**, 239 (1998).
[23] M. Peng, L. Wondraczek, Opt. Lett. **35**, 2544 (2010).
[24] M. Peng, J. Lei, L. Li, L. Wondraczek, Q. Zhang, and J. Qiu, J. Mater. Chem. C **1**, 5303, (2013).
[25] M. Yu. Sharonov, A. B. Bykov, V. Petricevic, and R. R. Alfano, Opt. Lett. **33**, 2131 (2008).
[26] M. Ping, G. Dong, L. Wondraczek, L. Zhang, N. Zhang, J. Qiu, J. Non-Cryst. Solids **357**, 2241 (2011).
[27] X. Fan, L. Su, G. Ren, X. Jiang, H. Xing, J. Xu, H. Tang, H. Li, L. Zheng, X. Qian, and H. Feng, Opt. Mat. Express **3**, 400 (2013).
[28] R. Gwin and R. B. Murray, Phys. Rev. **131**, 508 (1963).
[29] J-M Spaeth, W. Meise, and K. S. Song, J. Phys. Condens. Matter **6**, 3999 (1994).
[30] F. Seitz, J. Chem. Phys. **6**, 150 (1938).
[31] F. E. Williams, J. Chem. Phys. **19**, 457 (1951).
[32] R. S. Knox and D. L. Dexter, Phys. Rev. **104**, 1245 (1956).
[33] S. Sugano, J. Chem. Phys. **36**, 122 (1962).
[34] D. Bramanti, M. Mancini, and A. Ranfagni, Phys. Rev. B **3**, 3 (1971).
[35] J. Pejchal, E. Mihokova, M. Nikl, A. Novoselov, A. Yoshikawa, Opt. Mater. **31**, 1673 (2009)
[36] G. Kresse and J. Furthmüller, Phys. Rev. B **54**, 11169 (1996).
[37] G. Kresse and D. Joubert, Phys. Rev. B **59**, 1758 (1999).
[38] J. P. Perdew, K. Burke, and M. Ernzerhof, Phys. Rev. Lett. **77**, 3865, (1996).
[39] J. P. Perdew, M. Ernzerhof, and K. Burke, J. Chem. Phys. **105**, 9982 (1996).
[40] J. B. Varley, A. Janotti, C. Franchini, and C. G. Van de Walle, Phys. Rev. B 85, 081109(R) (2012).
[41] J. Paier, M. Marsman, K. Hummer, and G. Kresse, I. C. Gerber, J. G. Angyan, J. Chem. Phys. **124**, 154709 (2006).
[42] D. Muñoz Ramo, A. L. Shluger, J. L. Gavartin, and G. Bersuker, Phys. Rev. Lett. **99**, 155504 (2007).
[43] K. Biswas and M. –H. Du, Appl. Phys. Lett. **98**, 181913 (2011).
[44] M. -H. Du, J. Appl. Phys. **108**, 053506 (2010).
[45] M. -H. Du and S. B. Zhang, Phys. Rev. B **80**, 115217 (2009).
[46] M. –H. Du and K. Biswas, Phys. Rev. Lett. **106**, 115502 (2011).
[47] P. E. Blöchl, Phys. Rev. B **50**, 17953 (1994).
[48] S. Lany and A. Zunger, Phys. Rev. B **78**, 235104 (2008).
[49] S. –H. Wei, Comput. Mater. Sci. **30**, 337 (2004).
[50] C. G. Van de Walle and J. Neugebauer, J. Appl. Phys. **95**, 3851 (2004).
[51] M. P. Fontana and W. J. Sciver, Phys. Rev. 168, 960 (1968).
[52] R. M. Van Ginhoven, J. E. Jaffe, S. Kerisit, and K. M. Rosso, IEEE Trans. Nucl. Sci. **57**, 2303 (2010).
[53] S. Lany, Phys. Stat. Sol. B **248**, 1052 (2011).
[54] C. J. Delbecq, W. Hayes, and P. H. Yuster, Phys. Rev. **121**, 1043 (1961).
[55] M. -H. Du and D. J. Singh, Phys. Rev. B **81**, 144114 (2010).
[56] M. -H. Du and D. J. Singh, Phys. Rev. B **82**, 045203 (2010).
[57] K. P. Oboth, F. J. Lohmeier, and F. Fischer, phys. stat. sol. (b) **154**, 789 (1989).
[58] J. Pejchal, E. Mihokova, M. Nikl, A. Novoselov, A. Yoshikawa, Opt. Mater. **31**, 1673 (2009)
[59] H. F. Folkert, M. A. Hamstra, and G. Blasse, Chem. Phys. Lett. **135**, 246 (1995).
[60] I. Nicoara, M. Paraschiva, M. Stef, and F. Stef, Eur. Phys. J. B **85**, 292 (2012).
[61] L. K. Aminov, S. I. Nikitin, N. I. Silkin, A. A. Shakhov, R. V. Yusupov, R. Yu. Abdulsabirov, and S. L. Korableva, J. Phys.: Conden. Matter **18**, 4985 (2006).
[62] S. B. S. Sastry and S. M. M. Kennedy, phys. stat. sol. (a) **155**, 263 (1996).

[63] M. -H. Du and D. J. Singh, J. Appl. Phys. **112**, 123516 (2012).
[64] A. Canning, A. Chaudhry, R. Boutchko, and N. Grønbech-Jensen, Phys. Rev. B **83**, 125115 (2011).
[65] A. Bessiere, P. Dorenbos, C. van Eijk, K. Kramer, H. Gudel, C. Donega, and A. Meijerink, Nucl. Instrum. Methods Phys. Res. A **537**, 22 (2005).